COMPARISON OF SKY VIEW FACTOR ESTIMATES USING DIGITAL SURFACE MODELS

Bikalpa Adhikari

Submitted to the faculty of the University Graduate School
in partial fulfillment of the requirements
for the degree
Master of Science
in the Department of Geography,
Indiana University

February 2022

Accepted by the Graduate Faculty of Indiana University, in partial fulfillment of the requirements for the degree of Master of Science.

Master's Thesis Committee

_____

Jeffrey S. Wilson, Ph.D., Chair

_____

Owen J. Dwyer III, Ph.D.

_____

Aniruddha Banerjee, Ph.D.

_____

Bhuwan Thapa, Ph.D.

DEDICATION

This thesis is dedicated to my parents and to the Department of Geography, IUPUI who have supported me through the continuation of my education. Thank you very much for being a source of inspiration throughout my academic journey.

ACKNOWLEDGEMENT

First and foremost, I would like to express my deepest gratitude to Dr. Jeffrey Wilson for his guidance and support during my academic years at IUPUI and to the rest of my thesis committee members Dr. Owen Dwyer, Dr. Aniruddha Banerjee, and Dr. Bhuwan Thapa for constructive feedback and counsel. I also would like to thank Terri Crews for her administrative support along the way.

I wish to acknowledge all my friends and colleagues who are pursuing degrees in different parts of the world in diverse disciplines for their support in the process of completion of this thesis. A special thanks to two of my friends: Ohm Bhandari and Pratik Dhungana, for their motivation and willingness to discuss GIS research.

Finally, though there are many individuals who deserve their name mentioned, I conclude by expressing my deepest appreciation to my parents for always encouraging my work and sharing powerful life lessons.

Bikalpa Adhikari

COMPARISON OF SKY VIEW FACTOR ESTIMATES USING DIGITAL SURFACE MODELS

Better comprehension of the Urban Heat Island study requires information on the natural as well as built characteristics of the environment at high spatial resolution. Sky View Factor (SVF) has been distinguished as a significant parameter for Local Climate Zone (LCZ) classification based on environmental characteristics that influence the urban climate at finer spatial scales. The purpose of this thesis was to evaluate currently available data sources and methods for deriving continuous SVF estimates. The specific objectives were to summarize the characteristics of currently available digital surface models (DSMs) of the study region and to compare the results of using these models to estimate SVF with three different raster-based algorithms: Horizon Search Algorithm in R-programming (Doninck, 2018), Relief Visualization Toolbox (RVT) (Žiga et al., 2016), and the Urban Multi-scale Environmental Predictor (UMEP) plugin in QGIS (Lindberg, et al., 2018).

Jeffrey S. Wilson, Ph.D., Chair

Owen J. Dwyer III, Ph.D.

Aniruddha Banerjee, Ph.D.

Bhuwan Thapa, Ph.D.

TABLE OF CONTENTS

LIST OF TABLES

LIST OF FIGURES

INTRODUCTION

Human-induced changes to the physical properties of the Earth's surface are of particular concern in cities where complex urban morphology, high concentrations of anthropogenic heat emission sources, altered airflow patterns, and the prevalence of heat-absorbing materials interact to trap energy that contributes to the formation of Urban Heat Islands (UHIs) (Stone et al., 2001; Voogt and Oke, 2003). UHIs are defined as areas of higher temperature relative to neighbouring rural areas and can occur in the urban boundary layer above-average building height and in the urban canopy layer below roof level (Oke, 1995). Morphological properties of urban landscapes including building density, building surface area, and sky view factor affect energy exchange processes that contribute to the formation of UHIs, particularly in the urban canopy layer (Gál et al., 2007; Maoi, 2020). Because of their influence on local and micro-scale climatic processes, methods and data sources for deriving estimates of urban morphology are important considerations and an active area of research (Salamanca et al., 2011; Middel et al., 2018).

Sky View Factor (SVF) has been identified as an important urban morphology parameter because of its association with net long-wave radiation, which can be a primary driver of intra-urban air temperature variations and the formation of UHIs (Unger, 2009; Bernard et al., 2018; Dirksen et al., 2019). SVF is defined as "the ratio of radiation received by a planar surface from the sky to that received from the entire hemispheric radiating environment" (Watson & Johnson, 1987, p. 193). Calculated values of SVF can range from 0 for a location with no view of the sky, to 1 for a location free of all obstructions.

Low SVF in cities is characteristic of urban canyon floors surrounded by tall buildings that block the view of the sky and present increased surface area to reflect and absorb energy. This can lead to a net increase in heat storage and intensification of the UHI effect, especially at night when energy absorbed during the day is re-emitted. Conversely, high SVF values are indicative of locations with more open views of the sky that allow more heat energy to escape into the atmosphere (Oke, 1988; Svenson 2004; Dirsken et al., 2018). SVF has been shown to have a near-linear relationship with net long-wave radiation when measured at point locations on urban canyon floors and also when SVF measurements are aggregated to city blocks (Oke et al., 1981; Bernabé et al., 2018).

A variety of approaches for estimating SVF are available. Maio et al. (2020) identified several categories of SVF estimation methods including geometric measurements, fish-eye photographs, Global Positioning System (GPS) methods, simulations based on digital surface models (DSMs), and use of Google Street View imagery. Each of these methods has advantages and disadvantages and choosing a specific method can depend upon study area size and complexity, the desired precision of the estimates, data availability, and the number of measurements needed. In the case of model-based methods, availability and quality of existing data sources are important considerations, as is computational efficiency. For example, precise estimates of SVF can be derived using field-based hemispherical photographs captured with a fisheye lens pointing vertically upward (Grimmond et al., 2001; Matzarakis, A., & Matuschek, 2011). However, spatially continuous estimates of SVF for entire cities or larger areas require

more efficient approaches. For these applications, methods that rely on models in the form of raster or vector data offer a more practical approach.

As part of a broader initiative to develop geospatial data resources that facilitate the study of urban climate in the city of Indianapolis, Indiana and beyond, the purpose of this thesis was to evaluate currently available data sources and methods for deriving continuous SVF estimates. The specific objectives were to summarize the characteristics of currently available data sources that can be used to generate digital surface models (DSMs) of the study region, and to compare the results of using these models to estimate SVF with three different raster-based SVF estimation algorithms: Relief Visualization Toolbox (RVT) (Žiga et al., 2016), Horizon Search Algorithm in R-program (Doninck, 2018), and the Urban Multi-scale Environmental Predictor (UMEP) Plugin in QGIS (Lindberg, et al., 2018).

BACKGROUND

A common method for estimating SVF is the use of fisheye lens photography. For example, Debbage (2013) used a Nikon Coolpix camera equipped with a fisheye lens to compare SVF estimates collected in and around the city of Athens, Georgia. Photographs were taken in four different landscape settings including commercial, residential, downtown, and rural/open space. The magic wand tool in Adobe Photoshop was used to select visible sky portions of the photographs. SVF values were obtained by taking the ratio of the total number of pixels in the visible sky portion of the photograph to the total number of pixels representing the entire portion inside the fisheye lens. The results showed that SVF values were more heterogeneous in the downtown area where the mean Sky View Factor was 0.64. The lowest SVF value of 0.49 was associated with residential areas, which the authors attributed to denser tree canopy cover. While the fisheye photography method is relatively simple and easy to understand, challenges to this approach include the logistics of field sampling and, after the photos are collected, the need to adjust the selection of sky pixels during the classification process.

Other types of photographic technologies have been adapted for the estimation of SVF. One method has been explained in Middel et al. (2017) where a web-based tool simulates hemispherical fisheye photographs from Google StreetView imagery. SVF is estimated from the imagery using a modified Styen's method (Steyn et al., 1986; Chapman et al., 2001; Middel et al., 2017). This method involves the following mathematical equation:

$$\mathrm{SVF} = \frac{\pi}{2n}\sum_{i=1}^{n} sin\left(\frac{\pi(2i-1)}{2n}\right)\left(\frac{p_i}{t_i}\right)$$

Where *n* is the total number of circular rings, *i* denotes the ring for a particular iteration, and *pi/ti* is the ratio of the number of sky pixels to the number of pixels in the ring. In this method, each fisheye photograph is divided into *n* circular rings (default = 36) and the SVF is obtained by summation of the contribution by each circular ring from the equation above. An advantage of using Google Street View imagery is that it does not require DSMs for the area of interest. However, this method does require generating hemispherical photos from Google Street View and direct access to Google API for which good working knowledge of complex Python and JavaScript coding is needed. Another disadvantage to the Google Street View approach is that not every location has Street View imagery and, even if available, it is largely confined to views from the road. There can be many parts of a city that are not imaged.

In addition to photographic methods for the computation of SVF, various software has been developed to estimate SVF from DSMs. DSMs represent the elevation of the earth surface and natural and man-made objects, such as buildings and trees, on the surface. The Horizon package in R programming is an algorithm developed by Jasper Van Donnick (2018) to generate continuous SVF estimates from DSMs. This algorithm computes SVF within a maximum search distance for each of the pixels in a raster. The algorithm is based on the calculation and averaging of horizon elevation angles and SVF for a certain number of azimuth angles within a maximum search radius. Using higher values for search distances and the number of angles (directions) creates higher precision estimates, but at the cost of increased computational time.

Dirksen et al. (2019) used the Horizon package to compute SVF in Utrecht, Netherlands for locations characterized as grasslands, forests, and urban. SVF was estimated using DSMs with three different spatial resolutions (1m, 3m, and 5m) within varying radii and azimuth directions. The goal was to determine the optimal SVF estimation parameters for the study region. A significant variation was observed when comparing the SVF estimates derived from higher vs. coarser-resolution DSMs. The average SVF value from the 1m resolution DSM was 0.5, which changed to 0.7 and 0.8 with an increase in resolution to 3m and 5m, respectively. The authors noted that the 1m resolution DSM captured small alleys and patches of vegetation that were not modelled at coarser resolutions. Overall, the authors concluded that 1m or higher resolution DSMs were optimal, that using more than 16 azimuth search directions had no significant impact on SVF estimates, and that a maximum search radius of 100m was sufficient to capture important obstacles in the study region.

The software Relief Visualization Toolbox (RVT) was developed to compute several types of surface visualizations with raster based DEMs and DSMs (Žiga et al., 2016). RVT requires one or more raster inputs in a variety of formats within the Geospatial Data Abstraction Library (GDAL) such as JPEG, ASCII gridded XYZ, or GeoTiff. In addition to SVF, RVT also provides various techniques such as analytical hill shading and derivatives, positive and negative openness, slope relief models, and slope gradient. The software generates two types of SVF outputs: a 32-bit file that stores the full range of SVF values, and a simplified 8-bit, histogram-stretched GeoTiff that can be used for visualization purposes. RVT is free and relatively easy to use.

The SVF estimates from RVT can be utilized in various applications that consider the visualization of DEMs, DSMs, and automatic feature extraction for use in landscape archaeology, geomorphology, geology, hydrology, and forestry (Žiga et al., 2016). Zakšek et al. (2011) computed SVF using the RVT software and, similar to the study by Dirksen et al. (2019), compared how the number of search directions, maximum search radius, and spatial resolution of the input raster affected the results. The study focused on SVF as a technique for visualizing landscape features of cultural heritage significance, such as remnants of hill forts, defense walls, and archaic buildings. SVF rasters were created from a 0.5m resolution DEM covering an archaeological site in Slovenia. The researchers compared SVF generated using 8, 16, 32, and 64 search directions and search radii of 5, 10, and 20m. They concluded that SVF was significantly better than the more commonly used hill-shading visualization technique for highlighting features of importance in locations where the relief changed gradually. The authors noted that SVF enhanced the visual importance of the relative elevation of each point, as opposed to only the most prominent topographic features. While increasing the number of search directions beyond 16 had no significant visual effect, using a larger search radius was useful for emphasizing how features relate to the overall topographic surroundings, while smaller search radii emphasized local topographic importance.

The Urban Multi-Scale Environmental Predictor (UMEP) is an open-source software package that can operate as a standalone program or as a plugin for QGIS software. It provides a variety of tools for estimating morphological variables for urban climate research including SVF (Lindberg et al., 2018). UMEP's SVF tool takes a DSM or DEM as input and considers the azimuth and altitude of the sun at 655 locations spread

across the hemisphere to determine where shadows would be cast. In addition to the ground and buildings, UMEP allows incorporating vegetation canopy digital surface models. When adding vegetation canopy models to the process, it is necessary to specify the trunk height and the percentage of light that penetrates through the vegetation. Based on research by Konarska et al. (2013), the default value for light transmissivity through vegetation is set to 3.0%. Konstantinov et al. (2017) used the UMEP algorithm to calculate SVF based on a DSM covering the territory of the Moscow metropolitan area. There were significant variations in SVF values from 0.45 to 0.99 across the study area. As expected, the authors reported that the lowest values of SVF were characteristic of areas with dense high-rise buildings.

Local Climate Zones (LCZs) provide a research framework for the study of urban climate and for standardizing the worldwide exchange of geospatial data for urban climate modeling (Stewart & Oke, 2012). As previously mentioned, SVF is one of the important parameters for defining different LCZ types. There are 17 LCZ types including ten developed classes and seven natural classes. Six LCZ classes present in the downtown Indianapolis study area were examined in this thesis. In addition to SVF, other variables used in the LCZ classification system include building surface fraction, aspect ratio, roughness height, and impervious surface fraction. Previous research has shown that for each of the LCZ classes there is a standard range of parameters. The standard range of parameter values of SVF and other morphometric characteristics for the LCZ classes examined in this study are shown in Table 1.

Local Climate Zone (LCZ)	Sky View Factor (SVF)	Building Surface Fraction (%)	Aspect Ratio	Roughness Height (m)	Impervious Surface Fraction (%)
LCZ 1 Compact High-rise	0.2-0.4	40-60	>2	>25	40-60
LCZ 2 Compact Mid-rise	0.3-0.6	40-70	0.75-2	10-25	30-50
LCZ 3 Compact Low-rise	0.2-0.6	40-70	0.75-1.5	3-10	20-50
LCZ 5 Open Mid-rise	0.5-0.8	20-40	0.3-0.75	10-25	30-50
LCZ 6 Open Low-rise	0.6-0.9	20-40	0.3-0.75	3-10	30-50
LCZ 8 large Low-rise	>0.7	30-50	0.1-0.3	3-10	40-50

Table 1: Local Climate Zone Characteristics (Stewart and Oke, 2012) for zones examined in central Indianapolis

DATA AND METHODS

This study was carried out using surface elevation and building height data for the Indianapolis central business district and nearby areas. The study area is characterized by diverse urban morphology common to many modern cities. DSMs were created at 1m spatial resolution using bare earth data from the USGS 3D Elevation Program (3DEP) and building heights from four different sources: Microsoft (MS), OpenStreetMap (OSM), the American Institute of Architects (AIA), and LiDAR-derived building heights. Each of these building height sources is discussed below. The process for DSM creation followed the methods suggested by Gal et al. (2007) and (2009) as summarized in Figure 1. The fundamental idea of this method is to use the surface elevation from the USGS DEMs for areas not occupied by buildings and to add the height of buildings above the ground to the DEM where buildings occur.

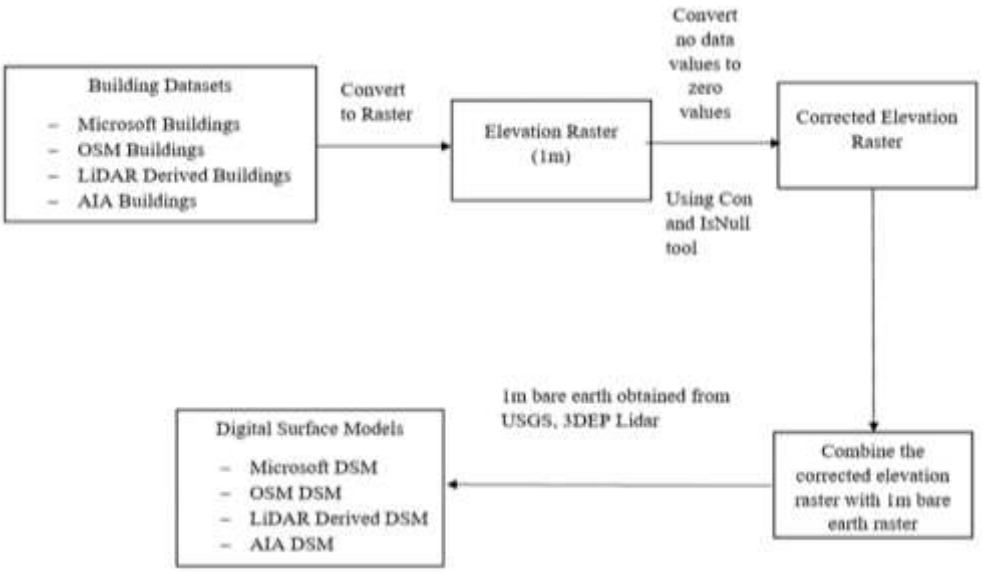

Figure 1: Workflow for creating Digital Surface Models (DSMs)

Building height Datasets

Microsoft buildings: In 2017, Microsoft released approximately 9.8 million building footprints for many metropolitan areas in 44 U.S. states. A year later, 125 million building footprints across most US states were released. For Indiana, the Microsoft building footprints available at the time of this research were limited to downtown Indianapolis and downtown Jeffersonville. Only the downtown Indianapolis building footprints were used. Details of the dataset used are summarized in Table 3. These building data are freely available for download at https://wiki.openstreetmap.org/wiki/Microsoft_Building_Footprint_Data.

OSM buildings: Footprints for an estimated 82% of the total buildings in the state of Indiana were obtained from OpenStreetMap. Around 18% of the total buildings obtained had no height information.

LiDAR-derived buildings: Using 2011 LiDAR, scholars from the School of Informatics, Computing and Engineering at Indiana University, Bloomington, Indiana created a building height dataset for Marion County, Indiana. The LiDAR points were used to estimate the average heights of 2D building footprints used to generate the corresponding DSM.

AIA buildings: In 2008, the American Institute of Architect (AIA) worked with Pictometry International Corp to create a 3D building model of central Indianapolis. The building model was designed using the Platinum 3D modelling tool implementing the methods described by Pictometry and Precision Lightworks (AIArchitect, 2008).

Table 2 summarizes the number of building footprints, their mean, minimum and maximum heights, and the number of the buildings without height information within the study region.

Building Datasets	Total number of Buildings	Maximum height (m)	Minimum height(m)	Mean height (m)	Number of Buildings with no height
MS Buildings	11586	220.49	5.53	13.46	0
OSM Buildings	19225	154	1.2	6.82	1483
LiDAR derived buildings	19116	356.764	6	18.2	0
AIA Buildings	3775	142.342	64.62	69.28	0

Table 2: Building footprints statistics for all the data sources.

The AIA building data were designed by engineers, planners, and architects with greater precision that exceeded the 2.5D extruded polygons that could be generated from the OSM, Microsoft, and LIDAR-derived datasets. The AIA model portrays a more realistic view of the buildings using an ESRI MultiPatch format that includes important 3D details such as different heights within the same building footprint and other architectural features. Figure 2 shows an example of the different building datasets for an area in the immediate vicinity of Pennsylvania Street and Georgia Street in downtown Indianapolis. A disadvantage of the AIA model compared to the other datasets is that it was based on data acquired prior to 2008 and is therefore outdated. For example, Figure 3 shows an area near the intersection of Kentucky Avenue and S West Street where buildings were demolished. In addition, the AIA data excludes a significant number of buildings that occur in the study area as illustrated by comparing building counts shown in Table 2.

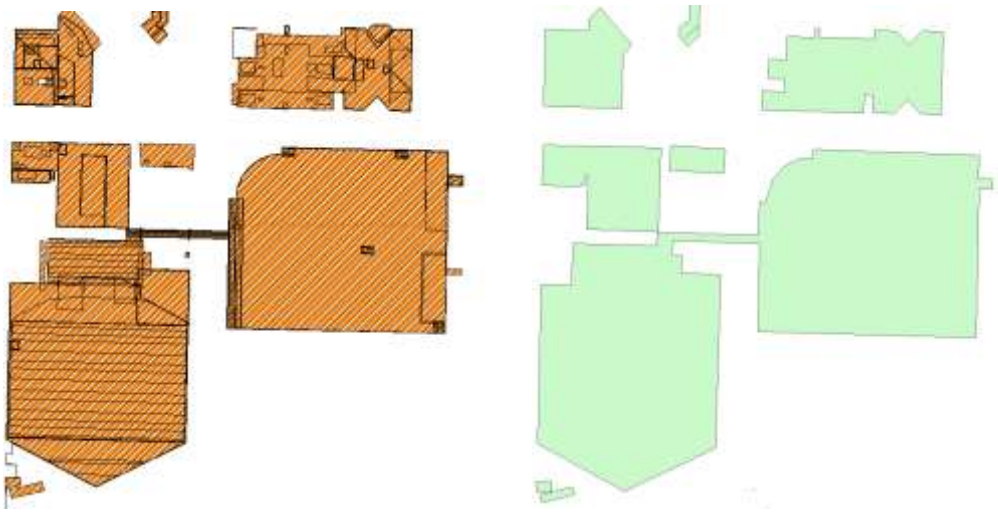

AIA Buildings Microsoft Buildings

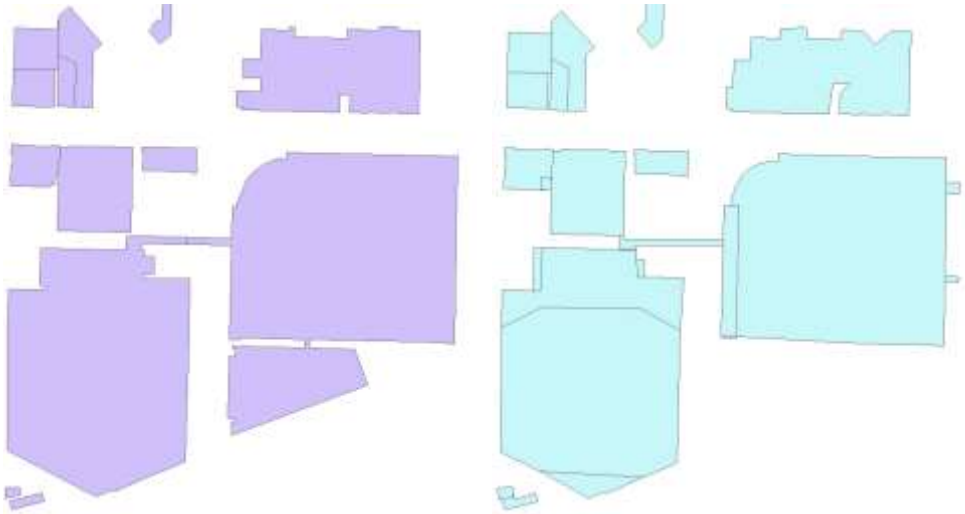

LiDAR derived Buildings OSM Buildings

Figure 2: Buildings near Pennsylvania Street and Georgia Street in downtown Indianapolis as modeled in the four different data sources.

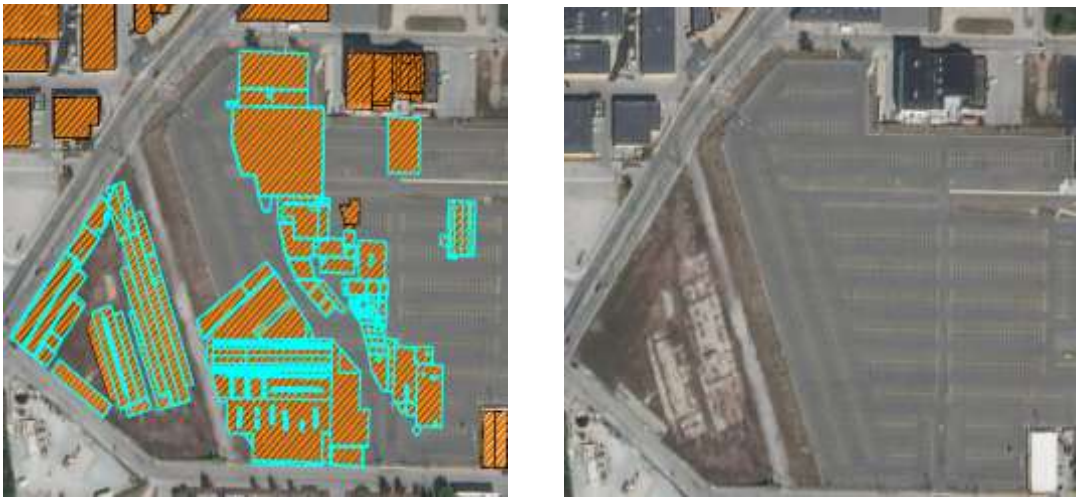

AIA Buildings (2008) Aerial Photograph (2020)

Figure 3: Buildings near the intersection of Kentucky Avenue and McCarty Street before (left) and after (right) demolition.

Polygons representing six different LCZ types present in the study region were digitized based on local knowledge of the urban landscape and visual interpretation of recent aerial photography (Figure 4). The polygons served as a basis for summarizing SVF estimates derived from the different DSMs and for comparison of the results to standard ranges used for LCZs as defined by Stewart and Oke (2012). The six LCZ types analysed in the study region included compact high rise, compact midrise, compact lowrise, open midrise, open lowrise, and large lowrise. Delineation of LCZ zones was limited to areas that had complete or near-complete building coverage in all four building height datasets.

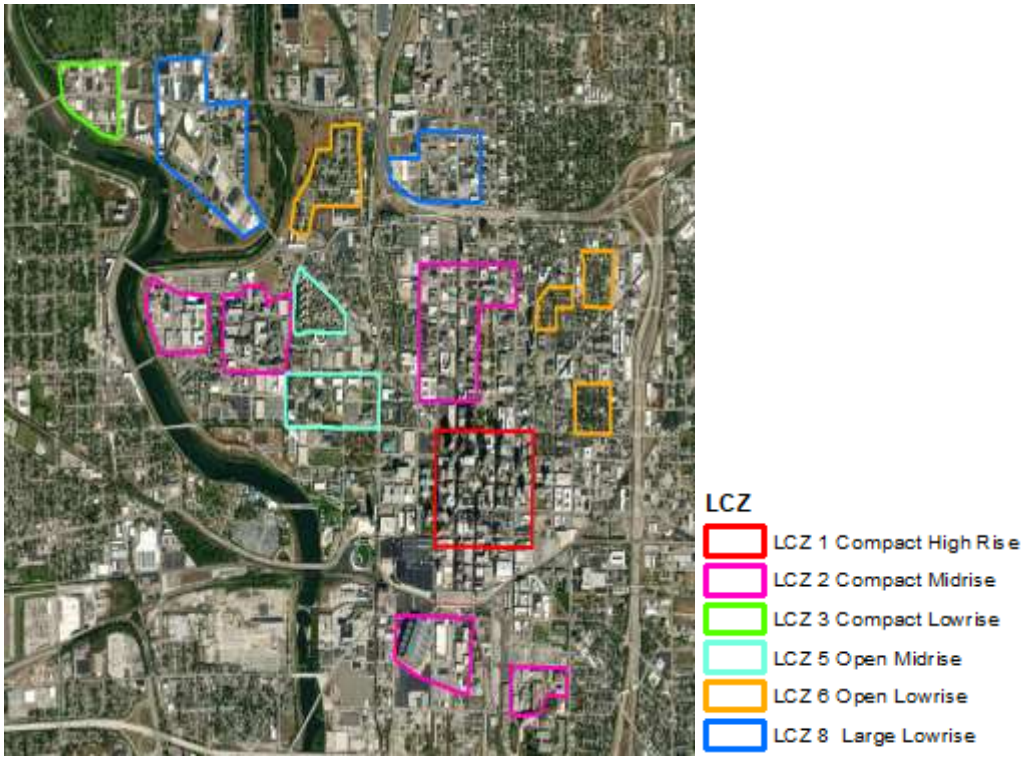

Figure 4: Local Climate Zone types identified in the central Indianapolis study area.

SVF estimates were created for the study region by processing each of the four DSMs using three different algorithms resulting in a total of twelve SVF raster outputs. The three algorithms used were Relief Visualization Toolbox (RVT) (Žiga et al., 2016), Horizon Search Algorithm in R (Doninck, 2018), and the Urban Multi-scale Environmental Predictor (UMEP) plugin for QGIS (Lindberg, et al., 2018). Both the RVT and Horizon algorithms require the analyst to specify the number of search directions and the maximum search radius when estimating SVF. In the current study, the number of directions was set to 16 and a maximum search distance of 500 meters was used based on the recommendations by Dirksen et al. (2019). The UMEP SVF tool does not require the user to choose a maximum search distance or set the number of azimuths, but it does offer the option to iterate the shadow casting algorithm for 145 or 655 times. The UMEP software documentation notes that the145-iteration setting produces SVF

images about three times faster, but the 655-iteration version was used in the current study to preserve the full precision of the method.

RESULTS

A subset of the DSMs derived by combining the USGS DEM data and each of the four building height sources is shown in Figure 5. The area depicted is centered on downtown Indianapolis and includes Lucas Oil Stadium slightly and Monument Circle. Table 4, 5, and 6 summarize basic descriptive statistics for each of the DSMs. The alphabetical symbols A, B and C in Figure 5 represent some of the conspicuous spots where there are differences in the DSMs due to absence or presence of buildings or differences that result from the limitations of 2.5D vs. 3D building height models. Figure 6 shows the SVF calculated from the four DSMs using the UMEP algorithm.

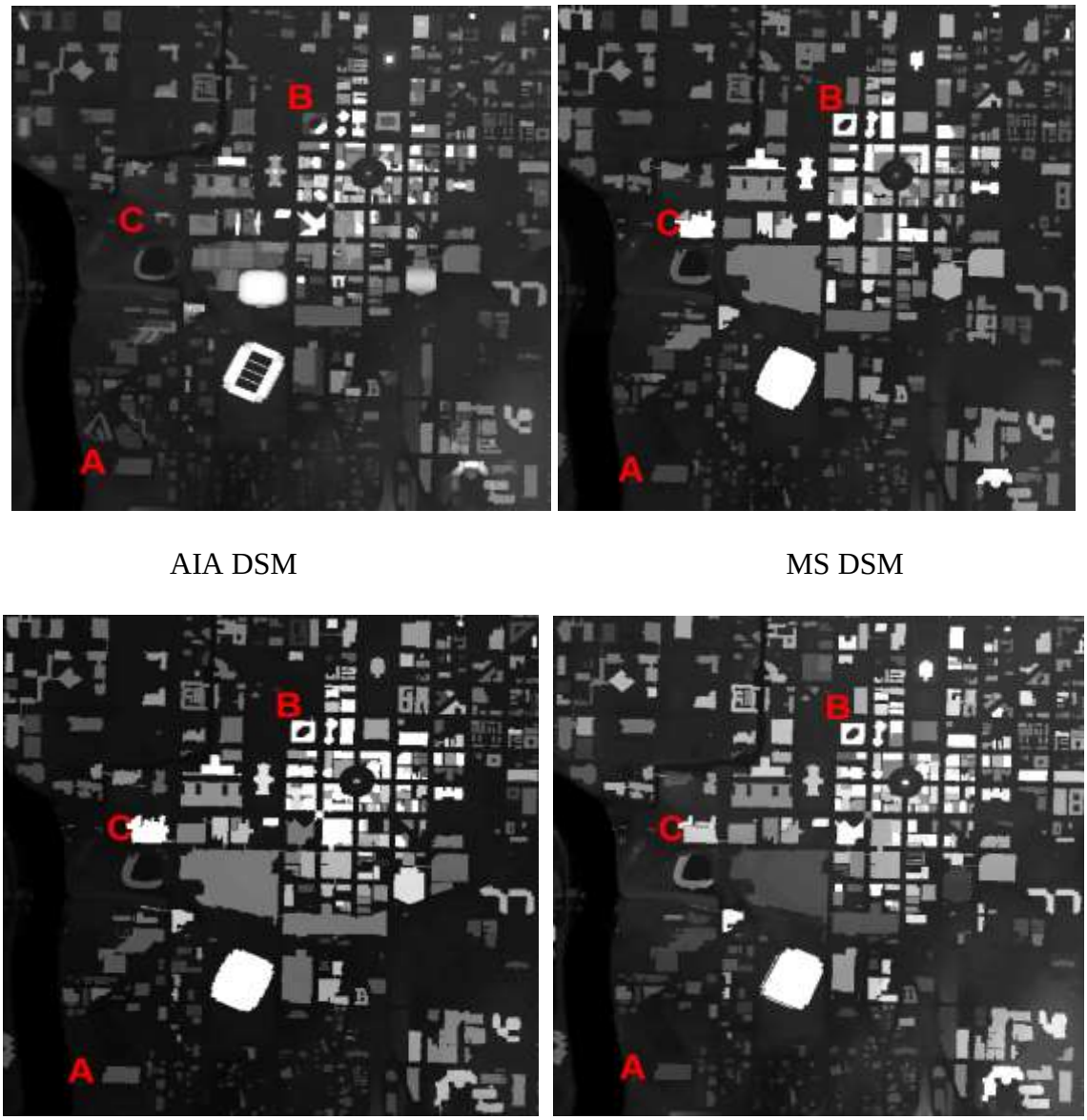

AIA DSM MS DSM

LiDAR DSM OSM DSM

Figure 5: Digital Surface Models (DSM) generated from four building height data sources for an area around Monument Circle in downtown Indianapolis.

DSM (↓)	Minimum	Maximum	Mean	Standard Deviation
MS DSM	203.08	439.3	219.11	11.81
OSM DSM	203.08	373.15	217.91	7.94
LiDAR derived DSM	203.08	573.82	221.51	18.95
AIA DSM	203.51	467.31	217.26	8.86

Table 3: Elevation and height statistics for the Digital Surface Models (DSMs).

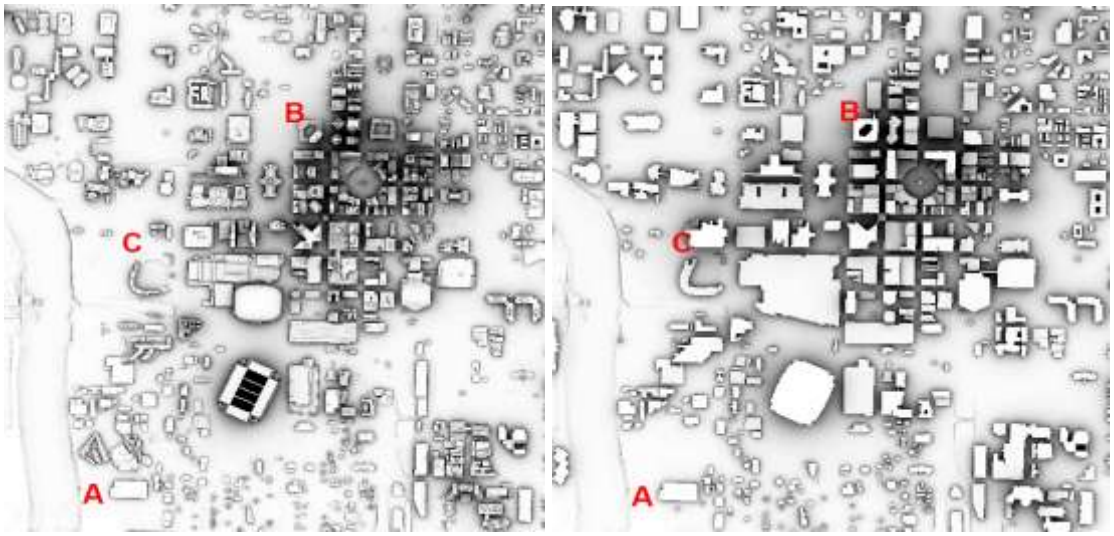

SVF (UMEP) for AIA DSM SVF (UMEP) for MS DSM

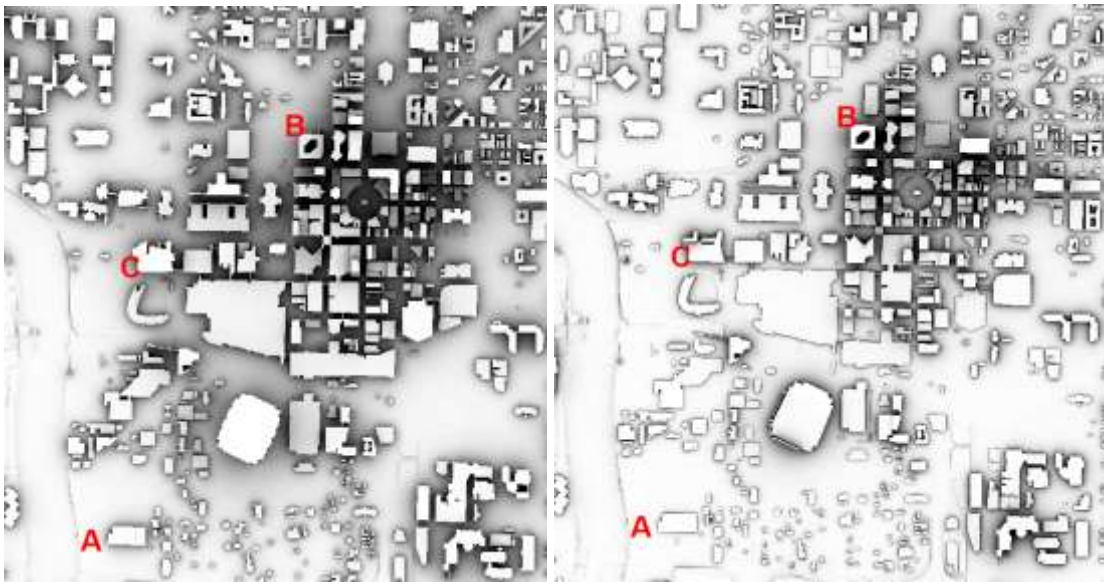

SVF (UMEP) for LiDAR DSM SVF (UMEP) for OSM DSM

Figure 6: Sky View Factor rasters for downtown Indianapolis derived using the UMEP algorithm and four different DSMs.

Data and Algorithm →	Relief Visualization Toolbox (RVT)			
Local Climate Zones (LCZ) ↓	OSM	MS	AIA	Lidar Derived
LCZ 1 (Compact High Rise)	0.614	0.569	0.624	0.498
LCZ 2 (Compact Mid Rise)	0.765	0.715	0.761	0.676
LCZ 3 (Compact Lowrise)	0.849	0.836	0.867	0.729
LCZ 5 (Open Midrise)	0.804	0.74	0.824	0.662
LCZ 6 (Open Lowrise)	0.749	0.636	0.766	0.568
LCZ 8 (Large Lowrise)	0.858	0.799	0.873	0.753

Table 4: Mean SVF values for six LCZ types across different DSM datasets using the RVT algorithm.

Data and Algorithm →	Urban Multiscale Environmental Predictor (UMEP)			
Local Climate Zones (LCZ) ↓	OSM	MS	AIA	Lidar Derived
LCZ 1 (Compact High Rise)	0.677	0.61	0.639	0.492
LCZ 2 (Compact Mid Rise)	0.843	0.784	0.827	0.721
LCZ 3 (Compact Lowrise)	0.927	0.91	0.935	0.821
LCZ 5 (Open Midrise)	0.887	0.821	0.887	0.722
LCZ 6 (Open Lowrise)	0.856	0.748	0.872	0.674
LCZ 8 (Large Lowrise)	0.93	0.88	0.935	0.827

Table 5: Mean SVF values for six LCZ types across different DSM datasets using the UMEP algorithm.

Data and Algorithm →	Horizon Package (R- Program)			
Local Climate Zones (LCZ) ↓	OSM	MS	AIA	Lidar Derived
LCZ 1 (Compact High Rise)	0.685	0.627	0.638	0.636
LCZ 2 (Compact Mid Rise)	0.834	0.779	0.816	0.729
LCZ 3 (Compact Lowrise)	0.918	0.901	0.928	0.807
LCZ 5 (Open Midrise)	0.882	0.819	0.882	0.731
LCZ 6 (Open Lowrise)	0.835	0.717	0.857	0.642
LCZ 8 (Large Lowrise)	0.924	0.873	0.931	0.825

Table 6: Mean SVF values for six LCZ types across different DSM datasets using the Horizon-Package algorithm.

Analytical procedures for comparing the results of SVF estimates developed by Hamerle et al. (2011) using Analysis of Variance (ANOVA) were adapted for the current study to determine whether there was significant difference between SVF estimates derived from the four different DSMs and the three different algorithms. The first ANOVA calculation tested if there was a significant difference in the SVF estimates across the three different DSM datasets using the UMEP algorithm in LCZ Class 1: Compact High Rise (LCZ 1). Since the algorithm and LCZ type were held constant, the ANOVA results provide insights into differences in the SVF estimates derived from the different DSMs. The second ANOVA focused on whether there was a significant difference between SVF estimates derived using the AIA DSM within all LCZ types but varying the SVF algorithms. Taking the ratio of the variation between samples and the variation within the sample provides an F statistic that follows the F-distribution. R programming is a well-known programming language for data analysis and statistical

computations. R-Studio was used in the current study to calculate the statistical parameters that were required for ANOVA. The following chart shows the workflow used for ANOVA calculation.

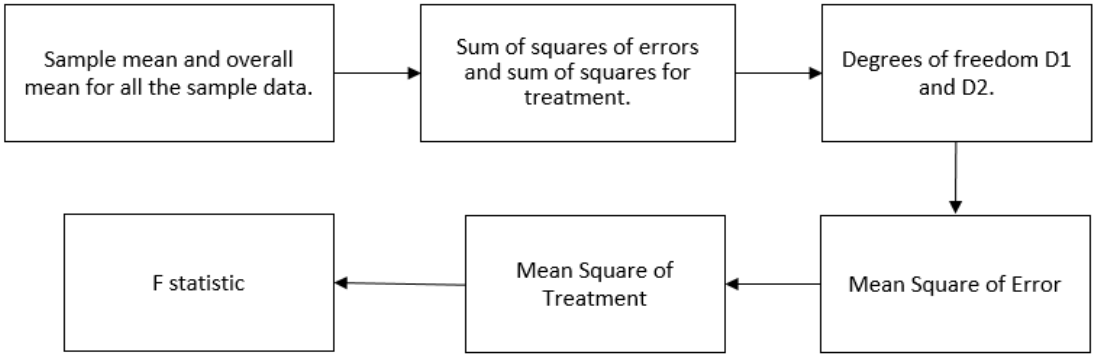

Figure 7: Workflow for ANOVA Calculation (Taylor, 2020).

The ANOVA calculation tested if there was a significant difference in the mean SVF across different DSM datasets and the mean SVF from UMEP algorithm in Local Climate Zone class - Compact High Rise (LCZ 1) as well as in all the zones irrespective of the LCZ class type. ANOVA was also used to examine whether the mean SVF values across different algorithms differed significantly when using the AIA dataset for LCZ 1 as well as in all the zones irrespective of the LCZ class type. The sum of squares of errors and the sum of squares of treatment were obtained using raster calculations in R. The degrees of freedom of error are given by the difference in the total count of pixels within the polygon and the number of groups. While running ANOVA in both scenarios mentioned above, the total pixel counts for LCZ1 as well as the total pixel counts for polygons representing all LCZ classes were noted from the zonal statistics and used in the computations accordingly.

There are two degrees of freedom in the first ANOVA, the degree of freedom of error and the degree of freedom of treatment. For the treatment, the degree of freedom is

given by: DF = n-1, where n is the number of groups. The degrees of freedom of error is given by the difference in the total count of pixels within the polygon and the number of observation groups. Tables 5 and 6 show the results generated.

ANOVA across 4 DSM datasets for UMEP algorithm

Extent	Sum of Squares of Errors	Sum of Squares of Treatment	Degree of Freedom (Error)	Degree of Freedom (treatment)	F Statistic
For LCZ 1	135393.323	0.019133	528047	3	0.0248
For all zones	1133709.899	0.04052	3379495	3	0.0405

Table 7: ANOVA results across the DSM groups using the UMEP algorithm.

ANOVA across 3 algorithms using the AIA DSM

Extent	Sum of Squares of Errors	Sum of Squares of Treatment	Degree of Freedom (Error)	Degree of Freedom (treatment)	F Statistic
For LCZ 1	71928.8	0.0028	528040	2	0.00093
For all zones	724553.273	0.00481	3379427	2	0.01122

Table 8: ANOVA results across the algorithm groups using the AIA DSM.

On placing the F-statistic to the F-distribution, the results were consistent with the null hypothesis of no significant difference in the mean SVF values across different DSM datasets using the UMEP algorithm. Similarly, no significant difference in SVF values across different algorithms using the AIA DSM was observed. The F- statistic was less than the F value in the F-distribution table with the 5% significance level for degree of

freedom (∞, 3) and (∞, 2). We can conclude that the evidence in the sample data we have is strong enough to stand by the null hypothesis for the whole population.

CONCLUSIONS AND FUTURE DIRECTIONS

The main objectives of this thesis were to explore different methods for the estimation of SVF in downtown Indianapolis and to compare different sources of building height data available for the study region. The findings show that several software packages have been developed in recent years for processing high-resolution raster-based digital surface models with reasonable hardware requirements and computational costs. This thesis demonstrated how digital surface models derived from four different sources can be used with three different algorithms to derive estimates of SVF. While the results obtained were specific to a portion of Indianapolis, the study area is representative of many modern cities and it's likely that similar results are obtainable for other locations and across larger geographic extents depending upon data availability. The findings from the thesis have allowed development of a better understanding of potential limitations based on the methods and sources used.

The greatest variations in the SVF estimates resulted from differences in the available building height datasets. Future work should focus on obtaining or developing a detailed 3D building model similar to that provided in the AIA dataset but updated to reflect current conditions and with more comprehensive coverage. This would provide more precise estimates of SVF by overcoming the limitations of 2.5D models such as those derived from the OSM, Microsoft, and LIDAR-based models that attribute simple 2D building footprints with a single height value. When comparing the four different algorithms, the UMEP approach appears to be more widely adopted in some of the leading urban climate studies. UMEP also provides the ability to integrate models of tree canopy in SVF calculations, which is necessary for deriving more realistic measures.

Future work could also be directed towards collecting field-based SVF estimates with fisheye lens photography at sampling locations in different local climate zone types to provide a basis for comparison with model-based estimates. If the focus of future work emphasizes thermal comfort at pedestrian/street levels, the buildings could be masked from the output raster to obtain ground-only values of SVF. The results of SVF estimates can also be integrated with field-based temperature sensors to validate the relationship between SVF and temperature in different settings. Similarly, SVF estimates could also be integrated with remote sensing-based estimates of land surface temperature (LST) such as those that can be derived from the Landsat or Sentinel series of Earth observation satellites.

REFERENCES

Bernabé, A., Bernard, J., Musy, M., Andrieu, H., Bocher, E., Calmet, I., Kéravec, P., & Rosant, J. M. (2015). Radiative and heat storage properties of the urban fabric derived from analysis of surface forms. Urban Climate, 12, 205-218.

Bernard, J., Bocher, E., Petit, G., & Palominos, S. (2018). Sky view factor calculation in urban context: computational performance and accuracy analysis of two open and free GIS tools. Climate, 6(3), 60.

Chapman, L. & Thornes, J. E. 2004. RealTime Sky-View Factor Calculation and Approximation. Journal of Atmospheric and Oceanic Technology, 21: 730–741.

Chapman, L., Thornes, J. E., Muller, J. P. & McMuldroch, S. 2007. Potential Applications of Thermal Fisheye Imagery in Urban Environments. Geoscience and Remote Sensing Letters, 4: 56–59.

Ching, Jason, G. Mills, Benjamin Bechtel, L. See, J. Feddema, X. Wang, C. Ren et al. "WUDAPT: An urban weather, climate, and environmental modeling infrastructure for the anthropocene." Bulletin of the American Meteorological Society 99, no. 9 (2018): 1907-1924.

Debbage, Neil. (2013). Sky-View Factor Estimation: A Case Study of Athens, Georgia. Geographical Bulletin - Gamma Theta Upsilon. 54. 49-57.

Dirksen, M., Ronda, R. J., Theeuwes, N. E., & Pagani, G. A. (2019). Sky view factor calculations and its application in urban heat island studies. Urban Climate, 30, 100498.

Fröhlich, D., Matzarakis, A., 2018: Spatial Estimation of Thermal Indices in Urban Areas-Basics of the SkyHelios Model. Atmosphere 2018, 9, 209, 1-14. doi:10.3390/atmos9060209.

Gal, T., Lindberg, F., & Unger, J. (2009). Computing continuous sky view factors using 3D urban raster and vector databases: comparison and application to urban climate. Theoretical and applied climatology, 95(1), 111-123.

Grimmond, C. S. B., Potter, S. K., Zutter, H. N., & Souch, C. (2001). Rapid methods to estimate sky-view factors applied to urban areas. International Journal of Climatology: A Journal of the Royal Meteorological Society, 21(7), 903-913.

Hämmerle, M., Gál, T., Unger, J., & Matzarakis, A. (2011). Comparison of models calculating the sky view factor used for urban climate investigations. Theoretical and Applied Climatology, 105(3), 521-527.

Hodul, M., Knudby, A., & Ho, H. C. (2016). Estimation of continuous urban sky view factor from Landsat data using shadow detection. Remote Sensing, 8(7), 568.

Jiao, Z. H., Ren, H., Mu, X., Zhao, J., Wang, T., & Dong, J. (2019). Evaluation of four sky view factor algorithms using digital surface and elevation model data. Earth and Space Science, 6(2), 222-237.

Johnson, G. T. & Watson, I. D. (1984) The determination of view-factors in urban canyons. J Climate Appl. Meterol. 23: 329–335.

Kidd, C. & Chapman, L. 2012. Derivation of Sky-View Factors from Lidar Data. International Journal of Remote Sensing, 33(11): 3640–3652.

Kokalj, Žiga & Zaksek, Klemen & Oštir, Krištof & Pehani, Peter & Čotar, Klemen. (2016). Relief Visualization Toolbox, version 1.3, Manual.

Konarska, Janina & Lindberg, Fredrik & Larsson, Annika & Thorsson, Sofia & Holmer, Björn. (2013). Transmissivity of solar radiation through crowns of single urban trees—application for outdoor thermal comfort modelling. Theoretical And Applied Climatology. 117. 1-14. 10.1007/s00704-013-1000-3.

Konstantinov, P. I., et al. "Shading areas, sky-view factor and UV radiation in urban canopy of Moscow city." AIP Conference Proceedings. Vol. 1810. No. 1. AIP Publishing LLC, 2017

Lindberg, F., & Grimmond, C. S. B. (2010). Continuous sky view factor maps from high resolution urban digital elevation models. Climate Research, 42(3), 177-183.

Lindberg F, Grimmond CSB, Gabey A, Huang B, Kent CW, Sun T, Theeuwes N, Järvi L, Ward H, Capel- Timms I, Chang YY, Jonsson P, Krave N, Liu D, Meyer D, Olofson F, Tan JG, Wästberg D, Xue L, Zhang Z (2018) Urban Multi-scale Environmental Predictor (UMEP) - An integrated tool for city-based climate services. Environmental Modelling and Software.99, 70-87 https://doi.org/10.1016/j.envsoft.2017.09.020

Matzarakis, A., Matuschek, O., 2011: Sky View Factor as a parameter in applied climatology - Rapid estimation by the SkyHelios Model. Meteorologische Zeitschrift 20, 39-45

Miao, C., Yu, S., Hu, Y., Zhang, H., He, X., & Chen, W. (2020). Review of methods used to estimate the sky view factor in urban street canyons. Building and Environment, 168, 106497.

Middel, A., Lukasczyk, J., Maciejewski, R., Demuzere, M., & Roth, M. (2018). Sky View Factor footprints for urban climate modelling. Urban climate, 25, 120-134.

Middel, Ariane & Lukasczyk, Jonas & Maciejewski, Ross. (2017). Sky View Factors from Synthetic Fisheye Photos for Thermal Comfort Routing—A Case Study in Phoenix, Arizona. Urban Planning. 2. 19. 10.17645/up. v2i1.855.

Mills, G., Ching, J., See, L., Bechtel, B., & Foley, M. (2015, July). An introduction to the WUDAPT project. In Proceedings of the 9th International Conference on Urban Climate, Toulouse, France (pp. 20-24).

M. Rafieian, H. R. Rad and A. Sharifi, "The necessity of using Sky View Factor in urban planning: A case study of Narmak neighborhood, Tehran," 2014 International Conference and Utility Exhibition on Green Energy for Sustainable Development (ICUE), 2014, pp. 1-5.

Oke, T. R. (1981). Canyon geometry and the nocturnal urban heat island: comparison of scale model and field observations. Journal of Climatology, 1(3), 237-254.

Rizwan, A. M., Dennis, L. Y., & Chunho, L. I. U. (2008). A review on the generation, determination and mitigation of Urban Heat Island. Journal of environmental sciences, 20(1), 120-128.

Salamanca, F., Martilli, A., Tewari, M., & Chen, F. (2011). A study of the urban boundary layer using different urban parameterizations and high-resolution urban canopy parameters with WRF. Journal of Applied Meteorology and Climatology, 50(5), 1107-1128.

Stone Jr, B., & Rodgers, M. O. (2001). Urban form and thermal efficiency: how the design of cities influences the urban heat island effect. American Planning Association. Journal of the American Planning Association, 67(2), 186.

Svensson, M. K. (2004). Sky view factor analysis–implications for urban air temperature differences. Meteorological Applications, 11(3), 201-211.

Taylor, Courtney. "Example of an ANOVA Calculation." ThoughtCo, Aug. 26, 2020, thoughtco.com/example-of-an-anova-calculation-3126404.

Unger, J. (2009). Connection between urban heat island and sky view factor approximated by a software tool on a 3D urban database. International Journal of Environment and Pollution, 36(1-3), 59-80.Voogt, J. A., & Oke, T. R. (2003). Thermal remote sensing of urban climates. Remote sensing of environment, 86(3), 370-384.

Watson, I. D., & Johnson, G. T. (1987). Graphical estimation of sky view-factors in urban environments. Journal of Climatology, 7(2), 193-197.

White, M., & Langenheim, N. (2014). Measuring urban canyons with real-time light based sky view factor modelling. In Our common future in urban morphology: 21st International Seminar on Urban Form: ISUF2014 (pp. 239-304).

Zhang, J., Gou, Z., Lu, Y., & Lin, P. (2019). The impact of sky view factor on thermal environments in urban parks in a subtropical coastal city of Australia. Urban Forestry & Urban Greening, 44, 126422.

CURRICULUM VITAE

Bikalpa Adhikari

EDUCATION

Master of Science — February 2022
Geographic Information Science (GIS)
Indiana University – Purdue University Indianapolis (IUPUI)
Indianapolis, Indiana

Bachelor of Engineering — December 2017
Geomatics Engineering
Tribhuvan University, Western Region Campus
Pokhara, Nepal

PROFESSIONAL EXPERIENCE

Graduate Research/Teaching Assistant — August 2019 – December 2021
Department of Geography, IUPUI
Indianapolis, Indiana

GIS and Cartographic Map Consultant Intern — June 2020 – July 2020
Indiana Trails
Indianapolis, Indiana

Geomatics Instructor — November 2018 – July 2019
Nepal Banepa Polytechnic Institute
Banepa-Kavre, Nepal

GIS and Remote Sensing Analyst — October 2017- November 2018
Sustainable Development and Research Centre
Kathmandu, Nepal

CONFERENCES/CERTIFICATIONS

Web GIS Development Course — February 2021
ArcGIS Web Maps with HTML, JS, CSS, and off the shelf tools — February 2021
West Lakes Division American Association of Geographers — November 2020
Social and Behavioral Responsible Conduct of Research — February 2020